Statistical uncertainty in background radiance measurements with single-photon detectors

Leonard Vollmann[a], Stefanie Häusler[a], and Florian Moll[a]

[a]German Aerospace Center (DLR), Institute of Communications and Navigation

ABSTRACT

Atmospheric background radiance is a critical factor in free-space Quantum Key Distribution (QKD) systems since it can significantly increase the Quantum Bit Error Rate (QBER). Accurate assessment of its impact on QKD requires measurements within the narrow spectral bandwidth and with detectors capable of sensing single photons used in QKD scenarios. These measurements serve as a valuable tool for site characterization, helping to asses the impact of background light at potential Quantum Optical Ground Station locations and to develop appropriate mitigation strategies. The single-photon detectors in the background light measurement setup need to be operated both at low detection rates at night and high detection rates by day. This is challenging because the dynamic range of sky background radiance spans roughly seven orders of magnitude. It is therefore crucial to accurately determine the statistical uncertainty of the photon rate measurements for incident background radiance of any intensity. Only then can a full error budget for the measurement results be confidently constructed. This contribution presents analytic results, obtained using Bayesian techniques, for the statistical uncertainty of rate measurements with realistic counting detectors including the effects of a finite detector dead time and a finite dark count rate. The effects of the after-pulsing probability and the detection efficiency are also discussed. In addition, these results give a formula for the measurement duration required to attain a given measurement accuracy, which can be used to optimize the 'hemisphere scan time' of a background radiance measurement instrument in real-time. The results are generic and can also be applied to other types of counting detectors, such as Geiger-Müller counters.

Keywords: Light pollution, background light, sky brightness, daylight QKD, Optical Ground Station, Quantum Key Distribution, SatQKD, Bayesian inference

1. INTRODUCTION

Accurate measurements of atmospheric background radiance are crucial for the construction of accurate error budgets for and the design of free-space QKD systems. The background photons are collected by the QKD receiver and contribute to increase the QBER. The intensity of atmospheric radiance depends on many factors: date and time of day, latitude, altitude, viewing direction, but also local atmospheric aerosol content, temperature, and ground albedo, among others. Theoretical and numerical investigations are possible, but accurate modeling would require measurements or accurate estimates of all of the relevant parameters. The direct measurement of atmospheric background radiance is therefore necessary in order to establish an experimental baseline with which other approaches can be validated in future.[1,2]

The sky background radiance is measured using single-photon detectors, in particular SNSPDs and SPADs. In order to accurately measure the day- and nighttime sky background radiance, these detectors need to be operated across their entire dynamic range, from a few counts per second to close to detector saturation. The evaluation of the statistical uncertainty in count rate measurements across this dynamic range is therefore crucial to the construction of an accurate error budget for the measurements.

We briefly describe the measurement setup that is considered in this contribution. It is shown in block-diagram form in figure 1. A fiber collimator is pointed in some direction into the sky (possibly on a moveable

Further author information: (Send correspondence to L.V.)
L.V.: leonard.vollmann@dlr.de
S.H.: stefanie.haeusler@dlr.de
F.M.: florian.moll@dlr.de

Environmental Effects on Light Propagation and Adaptive Systems VIII, edited by Karin Stein, Szymon Gladysz, Proc. of SPIE Vol. 13669, 136690I · 2025 Published by SPIE
0277-786X · doi: 10.1117/12.3077165

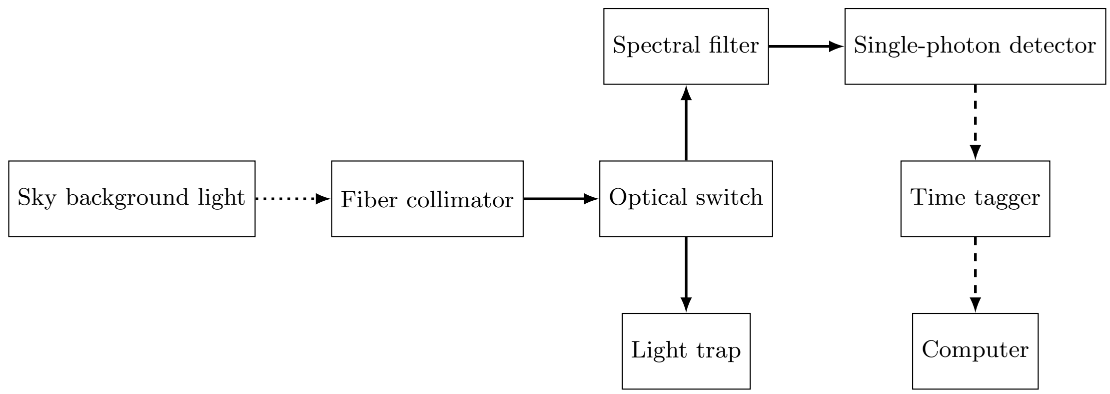

Figure 1. Block diagram of the measurement device.

mount to enable the scanning of the hemisphere at different viewing directions). The captured light is coupled into a single-mode fiber and, passing through an optical switch and spectral filter, is guided to a single-photon detector, typically a single-photon avalanche diodes (SPAD) or superconducting nanowire single-photon detectors (SNSPD). The detector clicks, in the form of electrical pulses, are recorded using a time tagger and a computer. The optical switch is used to close the detector to the incident sky background light, enabling the direct measurement of the detector's dark count rate.

The experiment proceeds as follows. The detector is opened to the sky for an amount of time T_0. The detector clicks comprise events caused by incident photons, dark counts, and after-pulses: This is the *signal measurement*. The recorded data is generally of the form of N numbers $\{n_i\}$ $(n_i \geq 0)$ associated with N intervals of temporal width δt_0. n_i is the number of detector clicks that have occurred in the ith interval. The total number of signal clicks is $n = \sum_i n_i$ and the total duration of the signal measurement is $T_0 = N\,\delta t_0$. The measurand is the *total* or *signal detector rate*, R. In addition to the signal measurement, a *noise measurement* is performed. The optical switch is closed and the detector clicks recorded for a time T_1. Now only dark counts are registered. Analogously to the signal measurement, the data is given by M intervals of temporal width δt_1 with associated counts $\{m_i\}$, with total counts $m = \sum_i m_i$ and $T_1 = M\delta t_1$. The measurand is the *dark count rate* R_d. The rate of detector clicks caused by incident photons (called *photon detection rate*) is thus obtained by subtracting the dark count rate from the signal rate:

$$R_\gamma = R - R_\mathrm{d}. \tag{1}$$

An ideal single-photon detector would generate exactly one electric pulse for every photon incident upon it, and no more. In reality, this is not the case. Several effects change the relationship between the number of photons absorbed by the detector and the number of detector clicks. We now briefly describe the most relevant of these effects.

Dark counts are detector clicks which occur without the incidence of a photon. The dark count rate is nonzero in real counting detectors such as SPADs and SNSPDs [3, Sec. 2.2.1] and must be included in calculations of measurement uncertainties, as it constitutes the noise floor above the signal of detector clicks caused by photons is to be measured.

The *dead time* T_d is the amount of time after each detector click during which no detection is possible. The maximum detector rate is $R_\mathrm{m} = 1/T_\mathrm{d}$. Since the detector is, in effect, closed for an amount of time T_d after each detector click, the actual time the detector is open during the measurement, T, is different from the total duration of the measurement T_0. The relation is $T = T_0 - nT_\mathrm{d}$, where n is the number of detector clicks. The total *event rate* $\tilde{R}$, defined in terms of T, is related to the detector rate R by:[1]

$$\tilde{R} = \frac{n}{T} = \frac{R}{1 - R/R_\mathrm{m}}. \tag{2}$$

This relation applies analogously to the photon rate: the *photon event rate* is

$$\tilde{R}_\gamma = \frac{R_\gamma}{1 - R_\gamma/R_\mathrm{m}}. \tag{3}$$

For $R \ll R_\mathrm{m}$, we have $\tilde{R} \simeq R$ to high accuracy. The detector is said to be in the *linear regime*. The inverse relation is

$$R = \frac{\tilde{R}}{1 + \tilde{R}/R_\mathrm{m}} \tag{4}$$

This is the detector response curve. We see that when the event rate grows large, $\tilde{R} \to \infty$, the detector rate saturates to $R \to R_\mathrm{m}$. In principle, we could extrapolate arbitrarily large event rates from the detector rate using the formula (2). We will see, however, that the statistical uncertainty $\Delta\tilde{R}^2$ of the event rate diverges near detector saturation. This results in a maximum detector rate beyond which the inference of the real event rate is no longer possible.

Any real detector has a *detection efficiency* $\eta < 1$, the probability of an absorbed photon to cause the detector to click. In order to relate this photon rate to irradiance measured by the instrument, one also needs to know the overall optical efficiency of the system, η_s. Thus the rate of photons which arrive at the detector is $R_\gamma = \eta^{-1}\eta_s^{-1}(R - R_\mathrm{d})$. These efficiencies also contribute to the photon rate measurement uncertainty. But this contribution is independent from the statistical uncertainties dealt with in this paper, as it solely stems from the uncertainty in the experimental measurement of η and η_s. We will therefore set $\eta = 1$ for the remainder of the paper in order to avoid clutter in the formulas.

After-pulsing is another effect which changes the relation between the detector rate and the corresponding physical event rate. For each detection event, there is a nonzero probability p_a of another click immediately following the dead time.[4] This means that each photon causes on average not one detector click (assuming perfect quantum efficiency), but

$$1 + p_\mathrm{a} + 2p_\mathrm{a}^2 + 3p_\mathrm{a}^3 + ... = 1 + \frac{p_\mathrm{a}}{(1 - p_\mathrm{a})^2} \tag{5}$$

detections (the probability of two after-pulses in a row is p_a^2, that of three is p_a^3, and so on). Thus the detector over-counts the amount of incident photons by the factor given in (5). Like the quantum efficiency, the after-pulsing probability can be neglected for the remainder of the considerations in this paper, since the its effect is statistically independent—the overall measurement uncertainty is only affected by the measurement uncertainty in p_a itself. The after-pulsing probability is related to the detector dead time: By setting a longer dead time on the detector, one generally achieves a lower after-pulsing probability.

The single-photon detectors need to be operated both at low detection rates at night and high detection rates by day in order to measure the background radiance in all regimes: The dynamic range of sky background radiance spans roughly seven orders of magnitude.[5] It is therefore crucial to accurately determine the statistical uncertainty of the photon rate measurements for incident background radiance of any intensity. That is, we wish to determine the variance $\Delta\tilde{R}_\gamma^2$ of the photon event rate (3) for any detector and dark count rate. We achieve this by invoking the method of Bayesian inference.

In section 2, we first consider the analysis of the measurement data using sample-based statistics. We show why this approach is unsatisfactory. We then apply the Bayesian formalism to two distinct regimes of measurement: the nonlinear and linear regime. When the photon rate is larger than the dark count rate (when measuring sky background radiance during the day), it is important to take into account the effects of the detector dead time and the resulting nonlinear detector response. The saturation of the detector leads to the divergence of the measurement uncertainties near the detector's maximum count rate. If the detector is assumed to respond linearly, the statistical moments of the relevant measured quantities can be computed exactly. Their behavior deviates from the asymptotic values at low count rates. The asymptotic results for large photon rates can be combined with the exact results for linear response, giving a formula for $\Delta\tilde{R}_\gamma^2$ that exhibits the correct behavior at low detector rates as well as the divergences associated with the dead time at high detector rates. From the results for the event rate variance $\Delta\tilde{R}^2$, one obtains an expression for the measurement duration T_0 required to attain a given measurement accuracy. These are the main results of this contribution.

After a summary of the results we show how they apply to the design of a background light measurement device.

2. STATISTICS OF RATE MEASUREMENTS

2.1 Sample-based statistics

First, consider a sample-based approach to the statistics of the experiment. Let the measured data of the first measurement be separated into N intervals of temporal width δt_0. Then, the sample means for the rates R and R_d are

$$\langle R \rangle = \frac{1}{N} \sum_{i=1}^{N} \frac{n_i}{\delta t_0} = \frac{n}{N \delta t_0} = \frac{n}{T_0} \tag{6}$$

and $\langle R_\mathrm{d} \rangle = m/T_1$, as expected. The sample variance of R is (including Bessel's correction)

$$\Delta R^2 = \frac{1}{N-1} \sum_{i=1}^{N} \left(\frac{n_i}{\delta t_0} - \langle R \rangle \right)^2 \tag{7}$$

and is bounded by $0 \leq \Delta R^2 \leq N \langle R \rangle^2$.* The results for ΔR_d^2 are analogous. Treating the measurements of R and R_d as independent, we arrive at the conclusion that the variance of the photon rate is $\Delta R_\gamma^2 = \Delta R^2 + \Delta R_\mathrm{d}^2$ and that it is bounded by

$$0 \leq \Delta R_\gamma^2 \leq N \langle R \rangle^2 + M \langle R_\mathrm{d} \rangle^2. \tag{8}$$

This is unsatisfactory for multiple reasons. For one, the results depend on the numbers of partitions N and M. By partitioning the measurement data in different ways, we obtain different sample variances. In addition, these relations overestimate the statistical uncertainty, as they treat the measurement of each n_i and each m_i as independent. They are not, since they correspond to the same (constant) physical event rate. Lastly, the measurements of R and R_d are also not independent, as the measurement of the total rate (dark counts + photons) implicitly includes a measurement of the dark count rate.

2.2 Bayesian rate inference

The formalism of Bayesian inference allows us to incorporate our knowledge of the physical nature of the system under investigation into the analysis of measurement data.[6] In particular, we would like to incorporate the fact that we are measuring events arriving at a constant rate, i.e., Poisson processes. The probability of n_i events to occur within the time interval δt_0, given the event rate R, is given by the Poisson distribution:

$$P(n_i|R) = \frac{(R\delta t_0)^{n_i}}{n_i!} e^{-R\delta t_0}. \tag{9}$$

This is called the *likelihood* of the occurrence of n_i events. The *prior* represents the knowledge of the rate prior to the experiment. In our case, the prior is the uniform distribution over the positive real numbers: $P(R) = 1$ (up to normalizing factor with the dimension of time). The marginalized likelihood is called the *evidence*. It is

$$P(n_i) = \int_0^\infty dR \, P(n_i|R) = \frac{1}{\delta t_0}. \tag{10}$$

Bayes' theorem now gives the *posterior* probability distribution for R as:

$$P(R|n_i) = \frac{P(n_i|R)P(R)}{P(n_i)} = \delta t_0 \frac{(R\delta t_0)^{n_i} e^{-R\delta t_0}}{n_i!}. \tag{11}$$

Given N values n_i, each corresponding to the number of events in time intervals δt_0, we have instead the likelihood

$$P(\{n_i\}|R) = \prod_{i=1}^{N} P(n_i|R) = \frac{(R\delta t_0)^n}{\prod_i n_i!} e^{-RT_0}, \tag{12}$$

*The lower bound occurs when the n_i are all equal, the upper bound corresponds to the situation in which all events occur during one of the intervals δt_0.

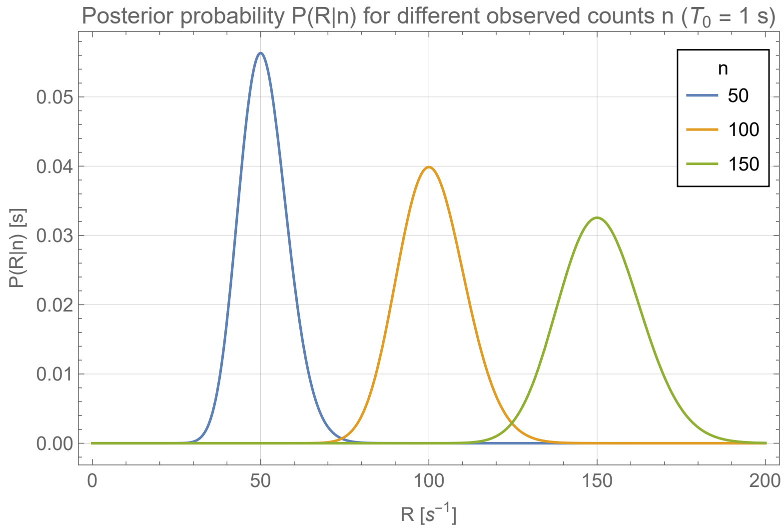

Figure 2. Posterior distribution $P(R|n)$ for different n and $T_0 = 1$.

where we have used $\sum_i n_i = n$ and $N\delta t_0 = T_0$. The evidence is $P(\{n_i\}) = \frac{\delta t_0^n}{T_0^{n+1}} \frac{n!}{\prod_i n_i!}$. Bayes' theorem then gives the inferred probability density for the rate given the observations $\{n_i\}$ as:

$$P(R|\{n_i\}) = P(R|n) = T_0 \frac{(RT_0)^n}{n!} e^{-RT_0}. \tag{13}$$

Figure 2 shows the posterior distribution for different values of the observed number of counts, n. Notice, in particular, that the distribution does not depend on the individual n_i, only on the total number of observed events, n. Thus the number of intervals N and the interval duration δt_0 do not matter—the total number of detections and the total time are enough to determine the posterior distribution. Consequently, the distribution's moments (the mean and variance) also only depend on n and T_0. This is in contrast to the sample-based approach, where the variance could be manipulated by re-partitioning the data.

The moments of the posterior distribution for R are $\langle R^k \rangle = T_0 \int_0^\infty dR\, R^k P(R|n)$. Substituting $x = RT_0$ and consulting an integral table, we find [7, Eq. 3.381.4]

$$\langle R^k \rangle = \frac{1}{T_0^k n!} \int_0^\infty dx\, x^{n+k} e^{-x} = \frac{1}{T_0^k} \frac{(n+k)!}{n!}. \tag{14}$$

The variance is thus

$$\Delta R^2 = \langle R^2 \rangle - \langle R \rangle^2 = \frac{(n+2)(n+1) - (n+1)^2}{T_0^2} = \frac{\langle R \rangle}{T_0}. \tag{15}$$

2.3 Inference of the photon detection rate

In order to determine the photon detection rate R_γ, we need to subtract the dark count rate R_d from the total rate R. In this section, we will calculate how the uncertainties in the signal and noise measurements combine in the uncertainty in R_γ. This is accomplished by constructing a hierarchical Bayesian model: the posterior in the first measurement will be used to construct the prior of the second measurement. In this way the implicit information about the dark count rate obtained in the measurement of the total rate is included, leading to a smaller statistical uncertainty.

We first determine the posterior probability distribution $P(R_\mathrm{d}|n, m)$ of the dark count rate given both the measurement of the full rate R and the dark count rate measurement. From $R = R_\gamma + R_\mathrm{d}$, we conclude that $R_\mathrm{d} \leq R$. The probability distribution of R_d given R is therefore $P(R_\mathrm{d}|R) = R^{-1}\theta(R - R_\mathrm{d})$, where θ is the Heaviside step function. This encodes the information obtained from the first measurement, namely that the dark count rate must be less than the total rate. From the first measurement we have $P(R|n)$, which gives [7, Eq. 3.381.3]

$$P(R_\mathrm{d}|n) = \int_0^\infty dR\, P(R_\mathrm{d}|R)P(R|n) = \frac{1}{n!}\int_{R_\mathrm{d}T_0}^\infty dx\, x^{n-1}e^{-x} = \frac{\Gamma(n, R_\mathrm{d}T_0)}{n!}, \tag{16}$$

where $\Gamma(n,x)$ is the upper incomplete gamma function. This, now, is the prior for R_d in the second measurement. The likelihood is computed to be $P(m|R_\mathrm{d}) = \frac{(R_\mathrm{d}T_1)}{m!}e^{-R_\mathrm{d}T_1}$.

We apply Bayes' theorem and find

$$P(R_\mathrm{d}|n,m) \propto P(m|R_\mathrm{d})P(R_\mathrm{d}|n) = \frac{\Gamma(n, R_\mathrm{d}T_0)}{n!}\frac{(R_\mathrm{d}T_1)^m}{m!}e^{-R_\mathrm{d}T_1}. \tag{17}$$

Substituting $x = R_\mathrm{d}T_0$ and $\alpha = T_1/T_0$, the normalization factor is obtained using the integral formula: [7, Eq. 6.455.1]

$$\int_0^\infty dx\, x^m \Gamma(n,x)e^{-\alpha x} = \frac{(m+n)!}{(m+1)}\frac{{}_2F_1(1, 1-n; m+2; -\alpha)}{(1+\alpha)^{n+m}}. \tag{18}$$

This gives

$$P(R_\mathrm{d}|n,m) = T_0\frac{m+1}{(m+n)!}\frac{(1+\alpha)^{n+m}}{{}_2F_1(1,1-n;m+2;-\alpha)}\,\Gamma(n, R_\mathrm{d}T_0)(R_\mathrm{d}T_0)^m e^{-\alpha R_\mathrm{d}T_0} \tag{19}$$

Now the joint posterior probability distribution for the photon and dark count rates is found by combining $P(R|n)$ and $P(R_\mathrm{d}|n,m)$ with the constraint that $R_\mathrm{d} + R_\gamma = R$:

$$P(R_\gamma, R_\mathrm{d}|n,m) = \int_0^\infty dR\, P(R|n)P(R_\mathrm{d}|n,m)\delta(R - R_\mathrm{d} - R_\gamma), \tag{20}$$

where δ is the Dirac delta function. Thus, with $x = R_\mathrm{d}T_0$ and $y = R_\gamma T_0$,

$$P(R_\gamma, R_\mathrm{d}|n,m) = T_0^2\frac{m+1}{n!(n+m)!}\frac{(1+\alpha)^{n+m}\alpha^m}{{}_2F_1(1,1-n;m+2;-\alpha)}(x+y)^n x^m\Gamma(n,x)e^{-x(1+\alpha)-y} \tag{21}$$

This is the inferred probability distribution: the joint distribution of the photon and dark count rates, given the data from the two measurements. The moments of this distribution are the results of the experiment, that is, the first and second moments give the predicted means and variances of R_d and R_γ.

There are two regimes to consider separately: $R_\gamma \gg R_\mathrm{d}$, when the nonlinear detector response needs to be taken into account and $R_\gamma \ll R_\mathrm{d}$, when the uncertainty in the measurement of the dark count rate dominates the overall uncertainty. These limits will be considered in turn.

2.4 Asymptotic calculation of the moments $\langle \tilde{R}_\gamma^k \rangle$ for high photon rates

If $R_\gamma \gg R_\mathrm{d}$ the two measurements decouple. This means that the information about R_d contained in the measurement of R is negligible. To see why, consider the kth moment of R_d w.r.t. the joint posterior:

$$\langle R_\mathrm{d}^k \rangle \propto \iint dx\, dy\, (x+y)^n x^{m+k}\Gamma(n,x)e^{-x(1+\alpha)-y} = \int_0^\infty dx\, x^{m+k}e^{-\alpha x}\,\Gamma(n,x)\Gamma(n+1,x), \tag{22}$$

where we evaluated the integral over y in terms of the incomplete gamma function. For large n, the function $\Gamma(n,x)\Gamma(n+1,x)$ is approximately constant for $x < n$ and falls quickly to zero around $x \simeq n$. The function $x^{m+k}e^{-\alpha x}$, in contrast, is peaked around $x = m/\alpha$. Thus, if $R_\gamma \gg R_\mathrm{d}$, the function $\Gamma(n,x)\Gamma(n+1,x)$ is constant when the function $x^{m+k}e^{-\alpha x}$ is non-negligible and does not contribute to the integral. We conclude from this that

$$P(R_\mathrm{d}|m,n) \simeq P(R_\mathrm{d}|m) = \frac{(R_\mathrm{d}T_1)^m}{m!}\,e^{-R_\mathrm{d}T_1} \tag{23}$$

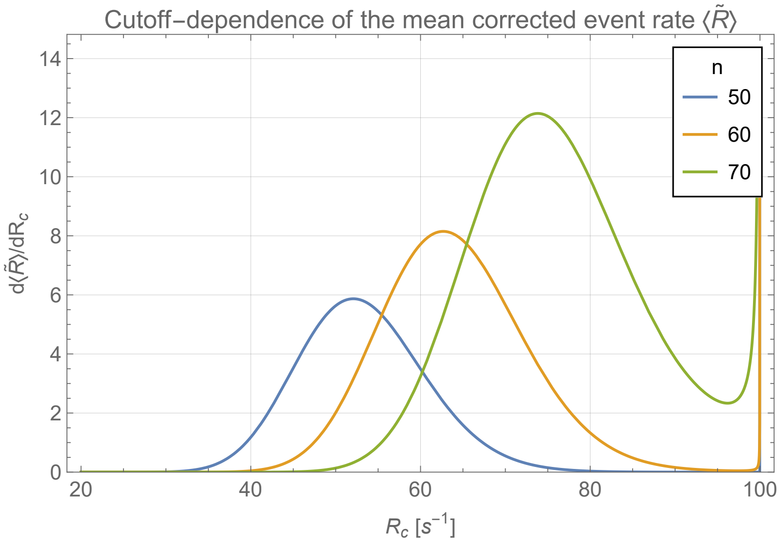

Figure 3. Influence of the cutoff R_c on the mean corrected event rate: $d\langle\tilde{R}\rangle/dR_\mathrm{c}$ for different n and $T_0 = 1$.

to sufficient accuracy. This means

$$\langle R_\gamma \rangle \simeq \langle R - R_\mathrm{d} \rangle = \frac{n+1}{T_0} - \frac{m+1}{T_0} \tag{24}$$

and

$$\Delta R_\gamma^2 = \Delta R^2 + \Delta R_\mathrm{d}^2 = \frac{n+1}{T_0^2} + \frac{m+1}{T_1^2} = \frac{\langle R_\gamma \rangle}{T_0} + \frac{T_0 + T_1}{T_0 T_1} \langle R_\mathrm{d} \rangle. \tag{25}$$

This is the *asymptotic* photon rate variance, valid for large R_γ.

The strength of the Bayesian formalism is that, having constructed the posterior probability distribution for R, we can compute the moments of any observable, i.e., function, of R. In particular, we are interested in the moments of the event rate $\tilde{R}$ (c.f. (2)):

$$\langle \tilde{R}^k \rangle = \int_0^\infty dR \left(\frac{R}{1 - R/R_\mathrm{m}} \right)^k P(R|n). \tag{26}$$

The integral diverges for all moments $k \geq 1$ because of the pole in the denominator. Physically, this is because the relation (2) maps the finite interval $R \in [0, R_\mathrm{m}]$ to the infinite interval $\tilde{R} \in [0, \infty)$, which causes the probability mass for all $R > R_\mathrm{m}$ to be concentrated near $R = R_\mathrm{m}$, making the expectation values divergent. In other words, the transformed probability distribution for $\tilde{R}$ is *fat-tailed*, since (2) allows for arbitrarily large R. Arbitrarily large photon rates are, of course, unphysical, so the solution is to regularize the integral by imposing a cut-off in the form of finite upper limit $R_\mathrm{c} < R_\mathrm{m}$ on the integral (26).

The cut-off must not affect the outcome of the measurement. We will see presently that this imposes an upper limit on the rate at which the detector may be operated—above this limit, an unambiguous inference of the real event rate is not possible. Consider the derivative of $\langle \tilde{R}^k \rangle$ with respect to the cutoff R_c:

$$\frac{d\langle \tilde{R}^k \rangle}{dR_\mathrm{c}} = \left(\frac{R_\mathrm{c}}{1 - R_\mathrm{c}/R_\mathrm{m}} \right)^k P(R_\mathrm{c}|n). \tag{27}$$

The posterior $P(R_\mathrm{c}|n)$ is peaked around $\langle R \rangle$ and has standard deviation of $\Delta R = \sqrt{\langle R \rangle / T_0}$ (c.f. (15)). The factor $R_\mathrm{c}/(1 - R_\mathrm{c}/R_\mathrm{m})$ diverges at $R = R_\mathrm{m}$. The measurement result is cutoff-independent if the derivative (27) vanishes. This is possible only if R_c is situated between the peak of the posterior and the pole at R_m. In particular, the peak and the pole must not overlap—in that case, there is no value of R_c at which the derivative vanishes. Figure 3 shows this: for $n = 70$, there is no R_c between the peak and R_m such that the derivative is (approximately) zero. The result of the measurement thus depends on the cutoff, rendering it unreliable.

Assuming we are operating in this regime, the cut-off integral for $\langle \tilde{R}^k \rangle$ can be evaluated using Laplace's method. We have, substituting $x = RT_0/n$,

$$\langle \tilde{R}^k \rangle = T_0^{-k} \frac{n^{k+n}}{n!} \int_0^{R_\mathrm{c} T_0/n} dx\, f(x)\, e^{-n\varphi(x)}, \tag{28}$$

where $f(x) = [x/(1 - nxT_\mathrm{d}/T_0)]^k$ and $\varphi(x) = x - \ln x$. The exponent $\varphi(x)$ has a maximum at $x_0 = 1$. Laplace's method works by expanding the integrand around the maximum of the exponent: with $\xi \equiv \sqrt{n}(x-1)$,

$$\begin{aligned} e^{-n\varphi(x)} &\simeq e^{-n\varphi(1) - \frac{1}{2}\varphi''(1)\xi^2 - \frac{1}{6\sqrt{n}}\varphi'''(1)\xi^3 - \frac{1}{24n}\varphi''''(1)\xi^4} \\ &\simeq e^{-n\varphi(1) - \frac{1}{2}\varphi''(1)\xi^2} \left(-\frac{1}{6\sqrt{n}}\varphi'''(1)\xi^3 - \frac{1}{24n}\varphi''''(1)\xi^4 + \frac{1}{72n}(\varphi'''(1))^2\xi^6 \right) \quad \text{and} \\ f(x) &\simeq f(1) + \frac{f'(1)}{\sqrt{n}}\xi + \frac{f''(x)}{2n}\xi^2, \end{aligned} \tag{29}$$

thus approximating the integral as a sum of Gaussian integrals

$$\begin{aligned} \int d\xi\, \xi^{2n} e^{-\frac{a}{2}\xi^2} &= \sqrt{\frac{2\pi}{a^{n+1}}}(2n-1)(2n-3)(2n-5)...(5)(3)(1), \\ \int d\xi\, \xi^{2n+1} &= 0 \quad \text{for } n = 0, 1, 2, 3.... \end{aligned} \tag{30}$$

For large n, Laplace's method thus gives [8, p. 273]

$$\langle \tilde{R}^k \rangle \simeq \frac{n^{k+n}}{T_0^k n!} \sqrt{\frac{2\pi}{n\varphi''(1)}} \left[f(1) + \frac{1}{n} \left(\frac{f''(1)}{2\varphi''(1)} - f(1)\frac{\varphi''''(1)}{8(\varphi''(1))^2} - f'(1)\frac{\varphi'''(1)}{2(\varphi''(1))^2} - f(1)\frac{5(\varphi'''(1))^2}{24(\varphi''(1))^3} \right) \right]. \tag{31}$$

Re-normalizing the moments by dividing by $\langle \tilde{R}^0 \rangle$ and expanding in powers of $1/n$, we find

$$\langle \tilde{R}^k \rangle \to \frac{\langle \tilde{R}^k \rangle}{\langle \tilde{R}^0 \rangle} = \left(\frac{\langle R \rangle}{1 - \langle R \rangle / R_\mathrm{m}} \right)^k \left(1 + \frac{k(k+1)}{2n(1 - \langle R \rangle / R_\mathrm{m})} + \mathcal{O}(\frac{1}{n^2}) \right). \tag{32}$$

Thus we have, to leading order in $1/n = 1/(\langle R \rangle T_0)$,

$$\begin{aligned} \langle \tilde{R} \rangle &\simeq \frac{\langle R \rangle}{1 - \langle R \rangle / R_\mathrm{m}}, \\ \Delta \tilde{R}^2 &\simeq \frac{\langle R \rangle / T_0}{(1 - \langle R \rangle / R_\mathrm{m})^3} = \frac{\Delta R^2}{(1 - \langle R \rangle / R_\mathrm{m})^3}. \end{aligned} \tag{33}$$

Thus the nonlinear response of the detector manifests itself in the appearance of the factor $(1 - \langle R \rangle / R_\mathrm{m})^{-3}$, which diverges as $R \to R_\mathrm{m}$. The photon event rate variance is thus

$$\Delta \tilde{R}_\gamma^2 = \frac{\Delta R^2}{(1 - \langle R \rangle / R_\mathrm{m})^3} + \Delta R_\mathrm{d}^2. \tag{34}$$

Note that we can easily solve for the measurement duration T_0 in (33):

$$T_0 = \frac{1}{\Delta \tilde{R}^2} \frac{\langle R \rangle}{(1 - \langle R \rangle / R_\mathrm{m})^3}. \tag{35}$$

This relation determines the measurement duration that is necessary to attain a given variance in the measurement of the event rate $\tilde{R}$ as a function of the detector rate.

2.5 Exact calculation of the moments $\langle R^k_{\gamma/d}\rangle$ (linear detector response)

We now calculate the moments $\langle R^k_\gamma\rangle$ and $\langle R^k_{\rm d}\rangle$ of the joint posterior probability distribution (20). Recall that these are the moments of the *detector rates* (without tildes). The results in this section thus apply to the *event rates* $\tilde{R}_{(\gamma)}$ provided the detector is operating in the linear regime, i.e., when $R \ll R_m$. Define $R_0 \equiv n/T_0$ and substitute the dimensionless integration variables $x = R_{\rm d}T_0$, $y = R_\gamma T_0$. Also define the parameter $\alpha = T_1/T_0$. This gives

$$\langle R^k_\gamma\rangle = \frac{1}{T_0^k}\frac{m+1}{n!(n+m)!}\frac{(1+\alpha)^{n+m}}{{}_2F_1(1,1-n;m+2;-\alpha)}I_k(n,m,\alpha), \tag{36}$$

and

$$\langle R^k_{\rm d}\rangle = \frac{1}{T_0^k}\frac{m+1}{n!(n+m)!}\frac{(1+\alpha)^{n+m}}{{}_2F_1(1,1-n;m+2;-\alpha)}I_0(n,m+k,\alpha) \tag{37}$$

where we have defined

$$I_k(n,m,\alpha) = \int_0^\infty dx\int_0^\infty dy\, y^k(x+y)^n x^m\Gamma(n,x)e^{-(x+y)-\alpha x}. \tag{38}$$

Using the integral representation of the incomplete gamma function [9, (8.6.5)], we write I_k as a triple integral:

$$I_k(n,\alpha,\beta) = \iiint dx\,dy\,dz\, x^{n+m}y^k(x+y)^n(1+z)^{n-1}e^{-(x+y)-\alpha x-x(1+z)}. \tag{39}$$

The calculation of moments thus amounts to the evaluation of the integral I_k. Fortunately, I_k is of a form that makes it amenable to evaluation via the *method of brackets.* This is a way of evaluating definite integrals based ultimately on Ramanujan's master theorem. It is a heuristic method which can be used to evaluate definite integrals which are intractable using other methods.[10,11]

We begin by writing the exponential as a power series:

$$e^{-(x+y)-\alpha x-x(1+z)} = \sum_{a=0}^{\infty}\phi_a\,[(x+y)+\alpha x+x(1+z)]^a. \tag{40}$$

where $\phi_a = (-1)^a/a!$ is called the *indicator*. The method of brackets tells us to assign to the expression $[...]^a$ the *bracket series*

$$[(x+y)-\alpha x-x(1+z)]^a = \sum_{b,c,d}\phi_b\phi_c\phi_d(x+y)^b(\alpha x)^c x^d(1+z)^d\frac{\langle b+c+d-a\rangle}{\Gamma(-a)}. \tag{41}$$

This assignment creates the terms $(x+y)^{n+b}$ and $(1+z)^{n-1+d}$ in the integrand. They are in turn assigned the bracket series

$$(x+y)^{n+b} = \sum_{e,f}\phi_e\phi_f x^e y^f\frac{\langle e+f-n-b\rangle}{\Gamma(-n-b)} \quad \text{and} \tag{42}$$

$$(1+z)^{n+d-1} = \sum_{g,h}\phi_g\phi_h z^g\frac{\langle g+h-n-d+1\rangle}{\Gamma(1-n-d)}. \tag{43}$$

The integral $\int dx x^a$ is assigned $\langle a+1\rangle$. Thus,

$$I_k = \sum_{a-h}\phi_{a-h}\frac{\alpha^c\langle n+m+c+d+e+1\rangle\langle k+f+1\rangle\langle g+1\rangle\langle b+c+d-a\rangle\langle e+f-n-b\rangle\langle g+h-n-d+1\rangle}{\Gamma(-a)\Gamma(-n-b)\Gamma(1-n-d)} \tag{44}$$

The bracket series is evaluated using the following rule:

$$\sum_{n_1,\dots,n_r}\phi_{n_1\dots n_r}f(n_1,\dots,n_r)\langle a_{11}n_1+a_{12}n_2+\dots+c_1\rangle\dots\langle a_{r1}n_1\dots+c_r\rangle = \frac{1}{|\det A|}f(n_1^*,\dots,n_r^*)\Gamma(-n_1^*)\dots\Gamma(-n_r^*). \tag{45}$$

The values n_i^* are the solutions to the linear system of equations obtained by requiring all bracketed expressions to vanish, i.e.,

$$\langle a_{11}n_1^* + a_{12}n_2^* + ... + c_r\rangle = ... = \langle a_{r1}n_1^* + a_{r2}n_2^* + ... + c_r\rangle = 0. \tag{46}$$

Applying this rule to (44), we find

$$I_k = k!\sum_i \phi_i \frac{(k-i+n)!}{(k-i)!}\sum_j \frac{(-\alpha)^j}{j!}\frac{\Gamma(m+1+i+j)\Gamma(n+m+1+i+j)}{\Gamma(m+2+i+j)} \tag{47}$$

The factorial in the denominator $(k-i)! = \infty$ for $i \geq 1+k$, so the sum over i terminates after $i = k$. In the inner sum, we recognize the series representation of the Gauss hypergeometric function ${}_2F_1$. We have, after applying Euler's transformation ${}_2F_1(a,b;c;x) = (1-x)^{c-a-b}\,{}_2F_1(c-a,c-b;c;x)$ [7, Eq. 9.131.1],

$$I_k = k!\sum_{i=0}^{k}\frac{(-1)^i(n+k-i)!(n+m+i)!}{i!(k-i)!(m+1+i)}\,\frac{{}_2F_1(1,1-n;m+2+i;-\alpha)}{(1+\alpha)^{m+n+i}}. \tag{48}$$

The moments are therefore

$$\langle R_\gamma^k\rangle = T_0^{-k}\sum_{i=0}^{k}\frac{(-1)^i(1+\alpha)^{-i}}{i!}\frac{k!}{(k-i)!}\frac{(n+k-i)!}{n!}\frac{(n+m+i)!}{(n+m)!}\frac{m+1}{m+1+i}\,G_i(n,m,\alpha), \tag{49}$$

and

$$\langle R_{\mathrm{d}}^k\rangle = \frac{1}{(T_0+T_1)^k}\frac{(n+m+k)!}{(n+m)!}\frac{m+1}{m+k+1}G_k(n,m,\alpha), \tag{50}$$

where G_i is the ratio of hypergeometric functions

$$G_i(n,m,\alpha) = \frac{{}_2F_1(1,1-n;m+2+i;-\alpha)}{{}_2F_1(1,1-n;m+2;-\alpha)} \tag{51}$$

We confirm that $\langle R_\gamma^0\rangle = \langle R_{\mathrm{d}}^0\rangle = 1$ as a sanity check. The first and second moments of the photon rate are

$$\begin{aligned}\langle R_\gamma\rangle &= \frac{n+1}{T_0} - \frac{n+m+1}{T_0+T_1}\frac{m+1}{m+2}G_1 \quad \text{and}\\ \langle R_\gamma^2\rangle &= \frac{(n+2)(n+1)}{T_0^2} - \frac{2(n+1)(m+n+1)}{T_0(T_0+T_1)}\frac{m+1}{m+2}\,G_1 + \frac{(m+n+2)(m+n+1)}{(T_0+T_1)^2}\frac{m+1}{m+3}\,G_2.\end{aligned} \tag{52}$$

The moments of the dark count rate R_{d} are

$$\begin{aligned}\langle R_{\mathrm{d}}\rangle &= \frac{n+m+1}{T_0+T_1}\frac{m+1}{m+2}G_1 \quad \text{and}\\ \langle R_{\mathrm{d}}^2\rangle &= \frac{(n+m+2)(n+m+1)}{(T_0+T_1)^2}\frac{m+1}{m+3}G_2.\end{aligned} \tag{53}$$

This gives

$$\Delta R_\gamma^2 = \frac{n+1}{T_0^2} + \frac{1}{(T_0+T_1)^2}\left((m+n+2)(m+n+1)\frac{m+1}{m+3}\,G_2 - (n+m+1)^2\frac{(m+1)^2}{(m+2)^2}G_1^2\right). \tag{54}$$

We recognize this to be the relation

$$\Delta R_\gamma^2 = \Delta R^2 + \Delta R_{\mathrm{d}}^2, \tag{55}$$

which provides another pleasant sanity check on the calculation. The dead-time corrected event rate variances are related to the detector rate variances by the relation (33). We conclude that the same relation holds here from the fact that the variance (54) converges to the asymptotic value (25) for large rates.[†] The variance of the photon event rate $\tilde{R}_\gamma$ is therefore

$$\Delta\tilde{R}_\gamma^2 = \frac{1}{(1-\langle R\rangle/R_\mathrm{m})^3}\frac{\langle R\rangle}{T_0} + \langle R_\mathrm{d}^2\rangle - \langle R_\mathrm{d}\rangle^2, \tag{56}$$

where the moments $\langle R_\mathrm{d}^k\rangle$ of the dark count rate are given by (53).

3. RESULTS AND DISCUSSION

The main results of this contribution are the expressions (25) and (56) for the statistical variance of photon event rate. The latter asymptotically approaches the former as the photon rate increases. The results were obtained using Bayesian inference of the rates of two measurements: One measuring the total detector rate (photons and dark counts, the signal measurement), one measuring only dark counts (the noise measurement). In addition, we obtained the relation (35), which gives the measurement duration required to attain a specified measurement accuracy.

Along the way, we found in section 2.2 that the statistics of the measurement only depend on the total number of observed detector events and the measurement duration (as well as the detector's parameters). The particularities of how the measurement device stores this information do not matter. This also means that the order in which the signal and the noise measurements are performed does not affect the outcome (the two could even be interleaved).

Further, we explained in section 2.4 that the measurement of high event rates using a detector with a finite dead time is only possible when the cutoff R_c does not affect the measurement, i.e., when the derivative (27) is negligibly small somewhere between its peak and the divergence at $R_\mathrm{c} \to R_\mathrm{m}$.

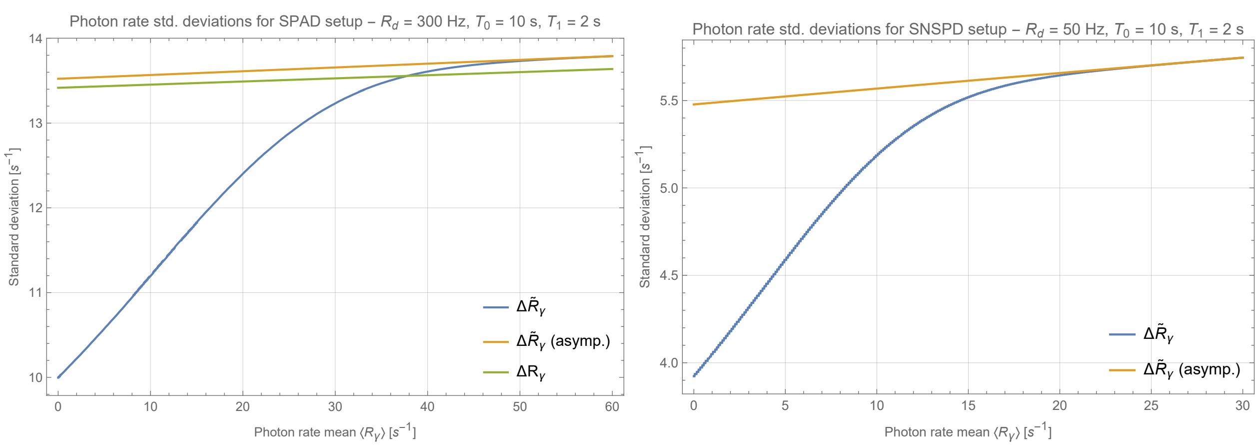

Figure 4. Left: photon rate uncertainty $\Delta\tilde{R}_\gamma$ (corrected) from (56) and (34), as well as the (uncorrected) uncertainty ΔR_γ for SPAD-like detector parameters. Right: corrected photon rate uncertainties for SNSPD-like detector parameters.

We now discuss how these results are applied to the system design of a background light measurement device. We begin by considering the regime of low detector rate. Figure 4 shows the standard deviations obtained from the results (56) and (34), as well as standard deviation without dead-time correction (25) for low photon rates. A plot each is given for a SPAD-typical parameters (with a dark count rate of 300 Hz and a dead time of 0.1 ms) and SNSPD-typical parameters (50 Hz dark count rate, 10 ns dead time). In both plots, $T_0 = 10\,\mathrm{s}$ and $T_1 = 2\,\mathrm{s}$. We see that the standard deviation based on the exact evaluation of the moments (56) deviates slightly from the asymptotic value for low photon rates. Crucially, the exact standard deviation of the photon event rate is as

[†]This can be explicitly calculated by applying Laplace's method to the three-dimensional integral (39). The calculation is omitted from the paper for reasons of brevity.

much as 30% smaller than the asymptotic formula (34) would estimate. This allows for the detection of photons even if the rate is only slightly above the noise floor.

The sensitivity (the minimum measurable photon event rate) of the device is determined mainly by the dark count rate of the detector. This can be seen in figure 4: the relative uncertainty falls below 100% at a mean photon rate of about 11 Hz and 5 Hz in the left and right plots, respectively. In order to achieve the best possible instrument sensitivity, a lower dark count rate should be prioritized in the system design. This is an important realization, since the detection efficiency η of single-photon detectors is typically related to the dark count rate: higher detection efficiency comes at the cost of higher dark count rate. The results of this analysis intimate that one should prioritize keeping the dark count rate as low as possible, possibly at the expense of the detection efficiency.

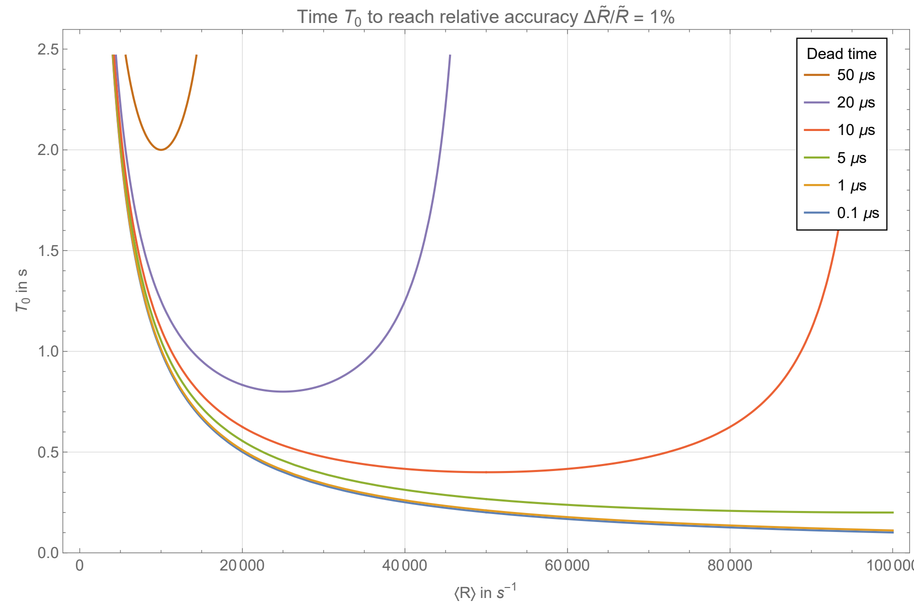

Figure 5. Measurement duration T_0 required to attain a relative dead-time corrected event rate uncertainty of $\Delta\tilde{R}/\tilde{R} = 1\%$ for dead times between $T_\mathrm{d} = 0.1\,\mu$s and $T_\mathrm{d} = 50\,\mu$s, as a function of the mean detector rate.

Figure 5 shows the effects of the detector non-linearity at high detector rates. The plot shows the measurement time T_0 required in order to obtain a relative error in the corrected event rate measurement of less than 1%. This is shown for different detector dead times. The required measurement duration is seen to diverge near the maximum detection rate $R_\mathrm{m} = 1/T_\mathrm{d}$. The divergence at zero is caused by the division by $\langle R \rangle$ in the *relative* measurement uncertainty.

These results impact the system design of a background light measurement device in multiple ways. A typical goal of a background light measurement is to obtain a 'brightness map'—the sky brightness as a function of the viewing direction. This could be realized by mounting the collimating optics on a movable mount and performing the measurement described in this paper is many times in sequence, pointing the collimator in different directions at the sky. Using the relation (35), such an instrument could, in real-time, calculate the necessary measurement duration for the current data point directly from the current detector rate, the dark count rate, and an accuracy goal. This way the instrument could consistently achieve the desired measurement accuracy efficiently, without measuring for longer than is necessary. In a 'brightness map'-measurement, where potentially hundreds of measurements are taken in sequence, this potentially saves a a considerable amount of time.

The consequence of the divergence of the measurement duration near detector saturation is that the dead time limits the maximum sky brightness measurable with the device. For daytime measurements, therefore, the detector dead time should be set as low as possible in order to extend the range of measurability. In addition, it may be advantageous to lower the detection efficiency, as this also decreases the detector rate caused by a given event rate.

The results of this paper are generic—the only assumptions are that the measured counts correspond to a Poisson process and that the detector has a finite dark count rate and dead time. Thus, one could apply the results straightforwardly to other types of counting detectors, such as Geiger-Müller counters.

4. CONCLUSION

In this contribution, we have demonstrated how Bayesian techniques can be used to conduct measurements of photon rates using single-photon detectors. Measurements of this kind are essential for site characterization in the context of free-space QKD ground stations. An accurate error budget of such measurements can only be constructed including sound knowledge and understanding of the underlying statistics. This is crucial if one wants to obtain reliable experimental results. The measurement scheme, consisting of two measurements—the *signal measurement*, which counts events caused by photons as well as dark counts, and the *noise measurement* in which only dark counts are registered—was shown to be simple enough to admit a fully analytic treatment. Assuming a linear detector response, the moments of the measurands (the photon and dark count rates) could be determined exactly, utilizing the so-called method of brackets, a heuristic analytical method, to evaluate the integrals. The nonlinear detector response caused by a finite detector dead time was dealt with using asymptotic techniques in the regime of large detection rates. The nonlinearity was shown to lead to a divergence of the measurands' moments as the detection rate approaches the maximum detector rate as determined by the dead time. These divergences, along with a condition of applicability of the asymptotic method (determined by the insensitivity of the results to an imposed cutoff), lead to the conclusion that, although arbitrarily large event rates can be inferred via the detector response curve from the detection rate, there is a limiting detection rate above which the statistical inference becomes meaningless. This limit is the upper edge of the envelope of event rates which are accurately measurable with a single-photon detector. The lower end of the envelope was shown to be determined by the detector's dark count rate: The statistical uncertainty of the dark count measurement determines the 'fuzziness' of the noise floor above which the background light signal is to be measured. Thus, the sensitivity of the instrument is largely determined by the dark count rate, while the maximum measurable event rate is determined by the dead time.

In order to create a 'map of sky brightness' with the measurement scheme described in this paper, it is necessary to perform said measurement many (possibly hundreds) of times in sequence, 'scanning' different viewing directions with the collimating optics. The result (35), which gives the measurement duration necessary to achieve a given measurement accuracy as a function of the current detection rate, allows the instrument to minimize the total scan duration in real-time.

The focus of this paper was on the statistics of the photon rate measurement. In the design of a measurement instrument, and the construction of a full error budget, this is only part of the story. Equally important are the uncertainties induced by the calibration, i.e., the measurement of the system parameters (the detector efficiency, optical system efficiency, dead time, after-pulsing probability). Each of these measurements adds to the overall rate measurement uncertainty. Their respective contributions are straightforward to take into account, however, as they do not depend on the measurement data. The results presented here may help lend the same kind of simplicity to the treatment of the statistics of photon rate measurement experiments.

ACKNOWLEDGMENTS

We thank Dr. Davide Orsucci for valuable comments and discussion, and gratefully acknowledge his thorough and insightful review of this report.

This report is based on projects funded by the German Federal Ministry of Research, Technology and Space under the funding code 16KIS1265 and by the European Space Agency (ESA) under the project "Background light and atmosphere metrology for QKD at urban locations" (BLAM). The authors are responsible for the content of this publication.

REFERENCES

[1] Häusler, S., Orsucci, D., Vollmann, L., Peev, E., and Moll, F., "Measurement-based characterization of atmospheric background light in satellite-to-ground quantum key distribution scenarios," *Optical Engineering* **63**(4), 041211–041211 (2024).

[2] Häusler, S., Schümann, F., Vollmann, L., Orsucci, D., Godin, P., Kuntz, K., Bayat, N., Jennewein, T., and Moll, F., "Measurements of atmospheric background light in the urban area waterloo and its impact on satellite qkd system performance," in [*Environmental Effects on Light Propagation and Adaptive Systems VII*], **13194**, 179–188, SPIE (2024).

[3] Chunnilall, C. J., Degiovanni, I. P., Kück, S., Müller, I., and Sinclair, A. G., "Metrology of single-photon sources and detectors: a review," *Optical Engineering* **53**(8), 081910–081910 (2014).

[4] Ziarkash, A. W., Joshi, S. K., Stipčević, M., and Ursin, R., "Comparative study of afterpulsing behavior and models in single photon counting avalanche photo diode detectors," *Scientific reports* **8**(1), 1–8 (2018).

[5] Er-long, M., Zheng-fu, H., Shun-sheng, G., Tao, Z., Da-sheng, D., and Guang-can, G., "Background noise of satellite-to-ground quantum key distribution," **7**(1), 215.

[6] Van de Schoot, R., Depaoli, S., King, R., Kramer, B., Märtens, K., Tadesse, M. G., Vannucci, M., Gelman, A., Veen, D., Willemsen, J., et al., "Bayesian statistics and modelling," *Nature Reviews Methods Primers* **1**(1), 1 (2021).

[7] Gradshteyn, I. S. and Ryzhik, I. M., [*Table of integrals, series, and products*], Academic press (2014).

[8] Bender, C. M. and Orszag, S. A., [*Advanced mathematical methods for scientists and engineers I: Asymptotic methods and perturbation theory*], Springer Science & Business Media (2013).

[9] "NIST Digital Library of Mathematical Functions." https://dlmf.nist.gov/, Release 1.2.4 of 2025-03-15. F. W. J. Olver, A. B. Olde Daalhuis, D. W. Lozier, B. I. Schneider, R. F. Boisvert, C. W. Clark, B. R. Miller, B. V. Saunders, H. S. Cohl, and M. A. McClain, eds.

[10] Gonzalez, I. and Moll, V. H., "Definite integrals by the method of brackets. part 1," *Advances in Applied Mathematics* **45**(1), 50–73 (2010).

[11] Gonzalez, I., Moll, V. H., and Straub, A., "The method of brackets. part 2: examples and applications," (2010).